Experimental Observation of Electron-Temperature-Gradient Turbulence in a Laboratory Plasma

S. K. Mattoo, S. K. Singh,[*] L. M. Awasthi, R. Singh, and P. K. Kaw

Institute for Plasma Research, Bhat, Gandhinagar-382 428, India

We report the observation of electron-temperature-gradient (ETG) driven turbulence in the laboratory plasma of a large volume plasma device. The removal of unutilized primary ionizing and nonthermal electrons from uniform density plasma and the imposition and control of the gradient in the electron temperature (∇T_e) are all achieved by placing a large (2 m diameter) magnetic electron energy filter in the middle of the device. In the dressed plasma, the observed ETG turbulence in the lower hybrid range of frequencies $\nu = (1\text{--}80 \text{ kHz})$ is characterized by a broadband with a power law. The mean wave number $k_\perp \rho_e = (0.1\text{--}0.2)$ satisfies the condition $k_\perp \rho_e \leq 1$, where ρ_e is the electron Larmor radius.

An understanding of electron transport across magnetic field lines in a fusion device is critical since in an ignited D-T fusion reactor the fusion alphas primarily heat electrons and typically, for reactor parameters, electrons and ions tend to be thermally equilibrated in general. Numerical simulations [1–4] and theoretical models [3–5] predict that electron-temperature-gradient (ETG) (∇T_e) driven ETG turbulence may be the main source for the observed anomalous electron thermal transport. ETG turbulence is a small-scale turbulence in magnetized plasma having a short wavelength, $k_\perp \rho_e \leq 1 \ll k_\perp \rho_i$, and low frequency, ω in the range $\Omega_i < \omega \ll \Omega_e$, where $k_\perp$ is the perpendicular wave vector, and ρ_e / Ω_e and ρ_i / Ω_i are the Larmor radii or gyro frequencies of electrons and ions. Linear calculations reveal that the ETG mode, which is responsible for the turbulence, is a fast growing instability driven by ∇T_e with growth rate $\gamma_{\text{ETG}} \approx \omega_{*Te} = k_y \rho_e (c_e / L_{Te})$, when $\eta_e = L_n / L_{Te}$ exceeds a threshold value. Here c_e is the electron thermal velocity and L_n and L_{Te} are the density and temperature gradient scale lengths, respectively. The conventional ETG instability is an electrostatic mode that arises in low beta plasma [6,7]; in high beta plasma, ETG becomes electromagnetic in nature [3,8,9].

Fluctuations on the electron gyroscale have been reported in the National Spherical Torus Experiment [10,11], and the role of ETG turbulence has been invoked to explain the plasma transport in Tore Supra [12]. However, not all of the signatures of ETG turbulence in these experiments could be obtained due to extremely small wavelength, $\rho_e \sim \mu$m in the range of $k_\perp \rho_e \sim 1$, in high magnetic fields (~ 20 kG) of tokamaks. Further, tokamaks have complex geometries, which restrict measurement and have limited control over the parameters that govern the turbulence. Basic plasma devices (linear or toroidal), on the other hand, provide a simplified geometry, a good realization of turbulence and control of some experimental parameters because they are operated at lower

plasma density and magnetic field to bring the scale length of turbulence into measurable limits [13]. Thus, there is a clear incentive to study ETG in basic plasma devices such as a large volume plasma device (LVPD). However, these devices usually have plasma, which is contaminated by the presence of ionizing, and hot and nonthermal electrons, which are potential sources of instabilities. This renders making a case for ETG difficult, as was faced by earlier attempts in a LVPD [14] and electron beam heating experiment [15].

A good experimental bed for studies on ETG should have no nonthermal electrons, a flat density profile, and a gradient in electron temperature. This ensures that instabilities driven by gradients in density and energetic electrons are not excited. In the past, attempts to produce such plasmas have not been successful. Establishing an independent control over density and temperature profiles has proved to be a difficult assignment. For example, heating electrons by injected electron beams have not yielded a convincing case for having experimentally observed ETG because beam electrons themselves are a potential source of instabilities. In this Letter, we report an unambiguous laboratory observation of ETG turbulence in the plasma of LVPD, devoid of nonthermal electrons. In this plasma, a suitable electron energy filter (EEF) filters out energetic electrons and allows imposition of a ∇T_e, keeping plasma density radially uniform.

The experiment is performed in a LVPD (Fig. 1, 2 m diameter, 3 m length, $P_0 \approx 10^{-6}$ Torr). The source of primary ionizing electrons is a set of 36 filaments (emission area ~ 75 cm^2), deployed on a 45 cm $\times$ 65 cm water-cooled rectangular plate cusped with 4 kG Sm$_2$CO$_5$ magnets. A similarly cusped end plate provides axial confinement of the plasma particles. The radial confinement of the plasma is provided by a uniform 6.2 G axial magnetic field.

A pulsed argon plasma is produced ($V_d \sim -70$ V, $I_d \sim$ 200 A, fill pressure of 10^{-4} Torr, $n_n \approx 10^{13}$ cm^{-3}) with
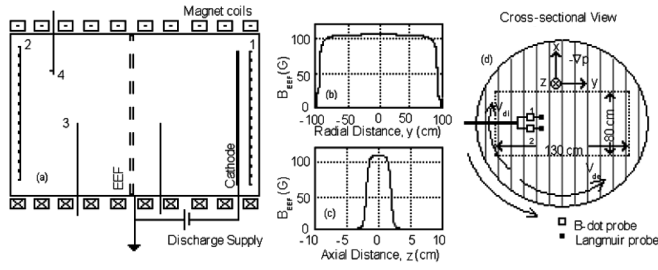
FIG. 1.   (a) The layout of the internal components of LVPD. The marked numbers represent, namely, (1) back plate, (2) end plate, (3) Langmuir probe, and (4) a pair of B-dot and Langmuir probes. (b),(c) The radial and axial magnetic field of EEF both along and across its axis and in cross-section view. (d) The dotted rectangular contour in this schematic shows the filament locations whereas vertical lines on it represent the coils of the solenoid.

$\Delta t_{\mathrm{discharge}} \sim 9.2$ ms [16]. The source consists of a cold population of high-density Maxwellian electrons ($n_{ec} \approx 3 \times 10^{11}$ cm^{-3}, $T_e \approx 3$ eV) and a low-density tail with energy <70 eV ($n_{e,\mathrm{tail}}/n_{ec} \approx 0.1$). Since energetic electrons in the source plasma have an isotropic distribution, the average parallel energy is 23 eV, 1/3 of the total energy ~ 70 eV. To remove the population of energetic electrons, we have introduced an electron energy filter. This filter is an 82% transparent solenoid with a rectangular cross section, which is placed on the diameter of the LVPD. Its cross section varies from (190 cm $\times$ 4 cm) at the axis of the LVPD to (4 cm $\times$ 4 cm) at the walls. We have observed that energetic electrons are trapped in the mirror of the solenoid field of the EEF on the source side of the LVPD. Hence, they are not found in the target region. The decrease in electron temperature is enabled by the velocity dependence of the particle transport of electrons across the magnetic field. The result is that the target plasma ($T_e \approx 1.8$ eV, $\beta_e \sim 0.2$–0.4) is devoid of energetic primary ionizing and nonthermal electrons [Fig. 2(a)]. Similar effects have been observed in a plasma produced in a cusp magnetic field [17]. Details of the EEF effects on transport of electron population through magnetic trapping and turbulence will be presented in a separate paper.
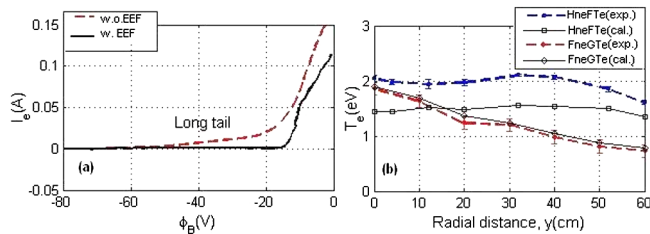

FIG. 2 (color online). I-V characteristics of Langmuir probe with EEF (w. EEF) and without EEF (w.o. EEF) are shown in (a) and a comparison of electron temperature in hollow and flat density plasma is made in (b).

Using measured values of the plasma potential ϕ_p and the floating potential ϕ_f from a pair of closely separated cylindrical Langmuir probes ($\Delta y \approx 2$ cm) aligned across the magnetic field in the relation $\phi_p = \phi_f + 5.4 T_e$ yields a measurement of T_e. Figure 2(b) shows a remarkable agreement between T_e determined by this formulation and that from the slope of the $I_e - V$ curve of the Langmuir probe. This verifies that energetic electrons have indeed been removed from the target plasma. A good agreement is not possible in the presence of energetic electrons in the plasma since they largely determine the floating potential.

The plasma parameters are measured with Langmuir probes and magnetic loops. The temperature fluctuations are estimated from $\delta T_e = e(\phi_2 - \phi_1)/\ln(I_{e1}/I_{e2})$ using two Langmuir probes where I_{e1}, I_{e2} are the electron currents at probe bias potential ϕ_1 and ϕ_2, respectively. A 16 channel guide user interface based VXI system (sampling rate ≤ 1 Gs/s) is used for data acquisition. The characteristics of turbulence are determined by using cross-correlation techniques.

Different combinations of radial profiles of the plasma parameters can be secured by resorting to different activation schemes of the EEF mainly by adjusting the physical size, magnitude, and spatial variation of the excitation current in the solenoid of the EEF. Figure 3 shows the radial profiles of the n_e, ϕ_p, T_e and temperature fluctuations for the selected two schemes used for experimental investigations of ETG. In the first scheme, the plasma is electric field free with flat plasma density and gradient in electron temperature (Fn$_e$GT$_e$) with typical scale length $L_{Te} \sim 50$ cm. In the second scheme, the plasma with hollow plasma density and no gradient in electron temperature (Hn$_e$FT$_e$) is embedded in a weak electric field with a reversal in the direction of the field at the point where gradient in plasma density changes sign. We define $r \leq 45$ cm as the core region and the remaining as the outer region with focus on the former. A consequence of gradient in electron temperature of the plasma is reflected in Fig. 3. About 13% of the fluctuations in electron temperature $\delta T_e/T_e$ are observed in the core plasma of Fn$_e$GT$_e$ and are conspicuously absent in Hn$_e$FT$_e$. Furthermore, in the Fn$_e$GT$_e$ about 2%–3% of fluctuations in plasma density ($\delta n_e/n_e$) and magnetic field ($\delta B_z/B_z$) are also excited. The δB_z appear only when the plasma beta ($\beta_e = 2\mu_0 n_e T_e/B_z^2$) exceeds a value $\beta_{e,cr} \sim 0.1$ (see Fig. 7). The plasma beta is controlled experimentally by varying discharge current through variation in filament temperature and has the effect of converting purely electrostatic fluctuations into partially electromagnetic ones. In the Hn$_e$FT$_e$ configuration, on the other hand, no fluctuations are observed in any of the plasma parameters. Even though the density gradient and velocity shear are present in Hn$_e$FT$_e$, the absence of gradient in electron temperature does not allow the ETG mode to get destabilized. The results from
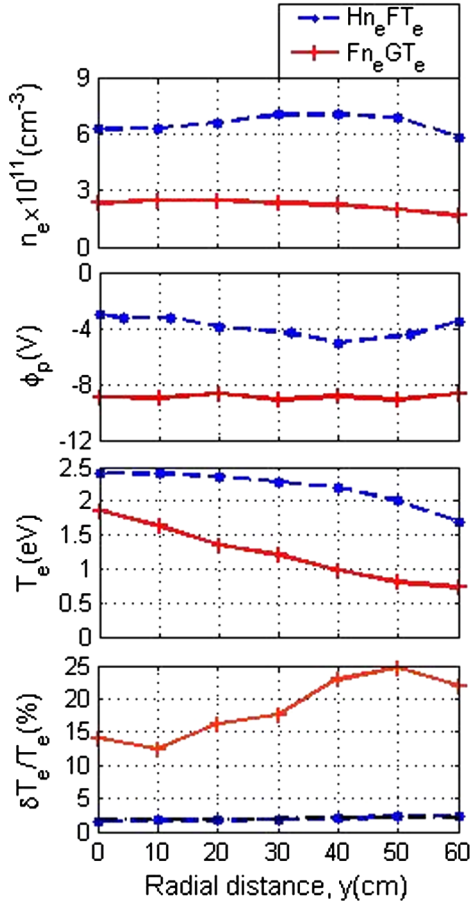
FIG. 3 (color online). Comparison of electron temperature fluctuations in hollow and flat density plasma is shown. A black dash-dotted line represents the noise.

FIG. 4 (color online).   (a) Frequency-power spectrum of δn_e, a similar spectra is seen for δB_z and δT_e, and (b) the cross-correlation functions.

simulation also show that hollow density and $E \times B$ velocity shear can destabilize the ETG mode for certain threshold conditions but only when $\nabla T_e < 0$ [18]. Thus we have clear empirical evidence for ∇T_e driven turbulence, which is electrostatic in low β_e plasma and gets coupled to an electromagnetic mode when the plasma β_e is high.

The observed turbulence exhibits broadband spectra with significant power between $\nu \lesssim 1$–15 kHz and a power law of $1/\nu^{1.8}$ for $\nu \lesssim 10$–80 kHz [Fig. 4(a)]. The observed mode frequency lies in the lower hybrid range of frequency $\Omega_i < 2\pi\nu \ll \Omega_e$, indicating that the basic instability driving the turbulence is that associated with the ETG mode. Strong evidence in favor of ETG mode identification is seen from cross-correlation functions between different fluctuating quantities [5], as shown in Fig. 4(b). Strong anticorrelation of $\delta n_e/n_e$ is observed with both $e\delta\phi/T_e(-0.8)$ and $\delta B_z/B_z(-0.7)$ and of $\delta T_e/T_e$ with $e\delta\phi/T_e(-0.7)$, respectively. The cross-correlation function of the same fluctuating quantity is measured by 4-probes at different axial positions. The phase shift observed corresponds to the poloidal velocity $V_{2,1} \approx 2.8 \times 10^3$ m/s,
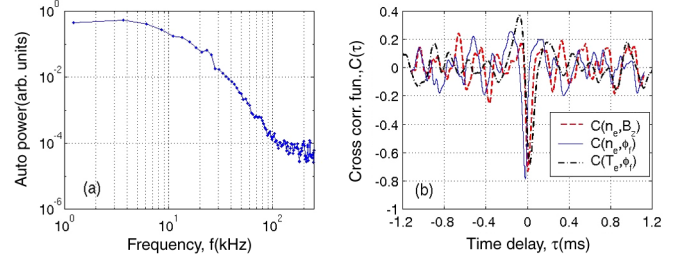
in the direction of electron diamagnetic drift velocity. The wave number frequency spectrum $S(k, \omega)$ exhibits peak power for both δn_e and δB_z at wave number $k_\perp \sim$ (0.1–0.3) cm^{-1} and frequency, $\nu \sim$ (1–5) kHz with spectrum width of $\Delta k/k \sim 2$ and $\Delta\nu/\nu \sim 2.5$, respectively [see Fig. 5]. A similar measurement is carried out for the parallel wave number and the typical values obtained are $k_\parallel \sim 0.008$ cm^{-1} with corresponding frequency, $\nu \sim$ 1–8 kHz. This satisfies the condition $k_\parallel/k_\perp \ll 1$ and thus exhibits a good agreement with the suggested theory for ETG turbulence.

We have thus experimentally demonstrated that in a plasma with Fn$_e$GT$_e$, the fluctuations in δT_e, δn_e, and δB_z exhibit strong signatures of electron-temperature-gradient driven turbulence. We now present a quantitative analysis of these experiments.

The frequency ordering of the ions in ETG dynamics is given by the expression $\Omega_i \sim \nu_{in} < \omega \le k_\perp c_i$, where $\Omega_i \sim 2 \times 10^3$ rad/s, $\nu_{in} \sim 3 \times 10^3$ s^{-1}, and $\omega \sim 2 \times 10^4$ rad/s are the ion gyro, ion-neutral collisional, and the characteristic frequency of the observed mode, respectively. The ions are considered as mobile, warm, collisionless, and unmagnetized. The physics of the ETG mode including the effects of δB_z, $\delta B_\perp$ perturbations and ion inertia is discussed in recent work by Singh et al. [9].
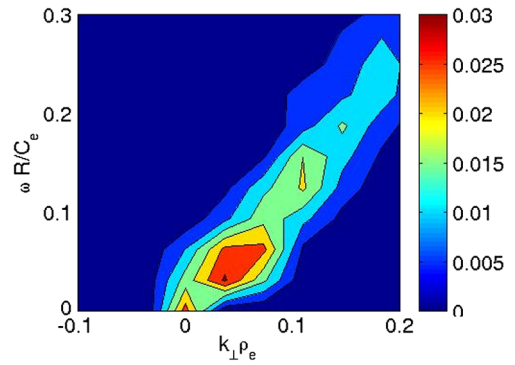

FIG. 5 (color online).   Contour plot of the joint wave number spectra for density fluctuations is shown with normalized parameters. This is at $y = 30$ cm and for $B_z = 5$ G. A similar spectrum is seen for δB_z.
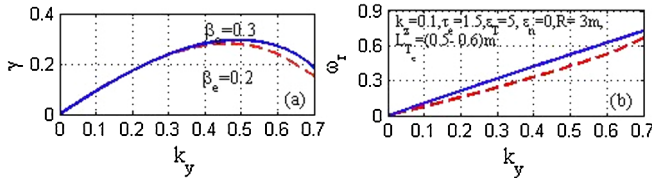
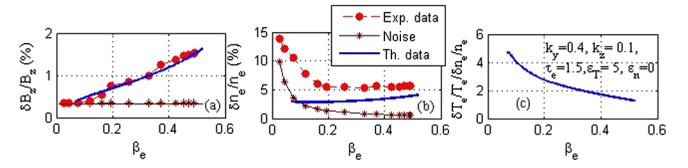FIG. 6 (color online).   Normalized (a) $\hat{\gamma}$ and (b) $\hat{\omega}_r$ versus $\hat{k}_\perp$ for ETG mode.

FIG. 7 (color online).   A comparison of the theoretically estimated and experimentally observed normalized fluctuations.

For $k_\perp L_{Te} \geq 3$ where bounded modes approach the WKB results, the generalized local dispersion relation for the ETG mode is given as

$$\hat{\omega}(\hat{\omega}\tau_e^* + \varepsilon_N \hat{k}_y + \hat{k}_\perp^2[\hat{\omega} - (\varepsilon_N + \varepsilon_T)\hat{k}_y]$$
$$+ \hat{\beta}(1 + \tau_e^*)\{\hat{\omega} - (\varepsilon_N + \varepsilon_T)\hat{k}_y\})$$
$$- \hat{\beta}[\hat{\omega} - (\varepsilon_N + \varepsilon_T)\hat{k}_y][(\varepsilon_T - 2\varepsilon_N/3)\hat{k}_y - 2\tau_e^*\hat{\omega}/3]$$
$$= \hat{k}_\parallel^2 \hat{k}_\perp^2 [(1 + 5\tau_e^*/3)\hat{\omega} - (\varepsilon_T - 2\varepsilon_N/3)\hat{k}_y]/[\hat{\omega}(\hat{\beta} + \hat{k}_\perp^2)$$
$$- \hat{\beta}(\varepsilon_N + \varepsilon_T)\hat{k}_y].$$

Here we have introduced normalized parameters: $\hat{\beta} = \beta_e/2$, $\varepsilon_T = R/L_T$, $\varepsilon_n = R/L_n$, $\hat{\omega} = R\omega/c_e$, $\hat{k}_\perp = \hat{k}_y \sim \hat{k}_x = k_\perp \rho_e$, $\hat{k}_z = k_z R = k_\parallel R$, $\hat{\rho}_e = \rho_{e/R}$, $\tau_e = T_e/T_i$, and $\tau_e^* = \tau_e[1 - \tau_e\hat{\omega}^2\hat{\rho}_e^2 m_i/\hat{k}_\perp^2 m_e]^{-1}$, where R is an arbitrary normalization length. From the above dispersion relation, the plots of linear growth rate ($\hat{\gamma}$) and real frequency ($\hat{\omega}$) versus $\hat{k}_\perp$ for different β_e keeping other parameters fixed are given in Fig. 6. It is found that the $\hat{\gamma}$ increases with the β_e value ($\beta_e \geq 0.1$) and has maximum growth at about $\hat{k}_\perp \approx 0.45$. The experimentally obtained normalized gradient $\eta_{e,\mathrm{expt}} \sim 6$ is found to be greater than the theoretical critical gradient for this plasma, $\eta_{e,\mathrm{theor}} \sim 1.5$ [9]. Note that the $E \times B$ rotation shear has a weak effect on the ETG mode since the shearing rate $dV_{E\times B}/dy \approx 0.04c_e/R$ is much smaller than growth rate of ETG mode in LVPD plasma.

To estimate the fluctuation levels at saturation, we note that for $k_\parallel/k_\perp \ll 1$, the perpendicular electron current $J_\perp = -en_e(v_{E\times B} + v_{*e})$ yields $\delta B_z/B = \tilde{B} \approx (\beta_e/2) \times (e\delta\phi/T_e - \delta p_e/p_{e0})$ and so the amplitudes of $\tilde{n}$, $\tilde{B}$, and $\tilde{T}$ can be expressed in terms of $\tilde{\phi}$ (using linear relations):

$$\langle \tilde{n} \rangle = -|\tau_e^*|\langle\tilde{\phi}\rangle,$$
$$\langle \tilde{B} \rangle = \hat{\beta}[1 + 5\tau_e^*/3] - (\varepsilon_T - 2\varepsilon_n/3)(\hat{k}_y/\hat{\omega})]|\langle\tilde{\phi}\rangle,$$
$$\langle \tilde{T} \rangle = |[(\varepsilon_T - 2\varepsilon_n/3)(\hat{k}_y/\hat{\omega}) - 2\tau_e^*/3]|\langle\tilde{\phi}\rangle.$$

We now approximate saturated values of $\tilde{\phi}$ using the mixing length estimates $\langle e\delta\phi/T_e\rangle \equiv \langle\tilde{\phi}\rangle \approx 1/k_x L_T = \hat{\rho}_e\varepsilon_T/\hat{k}_\perp$ [5]. Figures 7(a) and 7(b) show the variation of observed and theoretically estimated $\delta B_z/B_z$ and $\delta n_e/n_e$ along with noise as a function of β_e. This shows good agreement for β_e scaling. The ratio of theoretically estimated $\tilde{T}_e$ and $\tilde{n}_e$ amplitudes versus β_e are shown in

Fig. 7(c). For $\beta_e = 0.2$–0.3, the estimated value of $\tilde{T}_e \sim 12\%$ and is close to the experimental observations.

In summary, the experiments described here have provided an unambiguous demonstration of ETG driven turbulence in a magnetized laboratory plasma device. Several signatures of the observed turbulence have been shown to be consistent with theoretical predictions for finite beta ETG modes. These laboratory observations have significant implications for understanding electron transport in tokamak fusion plasmas. Although ETG instability of high beta plasma is not known to exist in present-day fusion plasmas, it may be important in alternate magnetic concepts [19–22]. They may also be relevant to such instabilities in a magnetospheric plasma during substorm activity, when the plasma beta is high [23]. Finally, the experiments showing the efficacy of the EEF are also relevant to the physics of negative ion formation and electron extraction in negative ion sources for high energy heating neutral beams [24].

*ssingh@ipr.res.in
[1] R. R. Parker, M. Greenwald, S. C. Luckhardt, E. S. Marmar, M. Porkolab, and S. M. Wolfe, Nucl. Fusion **25**, 1127 (1985).
[2] R. J. Goldston, Plasma Phys. Controlled Fusion **26**, 87 (1984).
[3] F. Jenko and W. Dorland, Phys. Rev. Lett. **89**, 225001 (2002).
[4] W. M. Nevins, J. Candy, S. Cowley *et al.*, Phys. Plasmas **13**, 122306 (2006).
[5] R. Singh, P. K. Kaw, and J. Weiland, Nucl. Fusion **41**, 1219 (2001).
[6] C. Holland and P. H. Diamond, Phys. Plasmas **9**, 3857 (2002).
[7] P. N. Guzdar, C. S. Liu, J. Q. Dong, and Y. C. Lee, Phys. Rev. Lett. **57**, 2818 (1986).
[8] R. Singh, V. Tangri, H. Nordman, and J. Weiland, Phys. Plasmas **8**, 4340 (2001).
[9] S. K. Singh, L. M. Awasthi, R. Singh, P. K. Kaw, R. Jha, and S. K. Mattoo, Phys. Plasmas **18**, 102109 (2011).
[10] E. Mazzucato *et al.*, Phys. Rev. Lett. **101**, 075001 (2008).
[11] Y. Ren *et al.*, Phys. Rev. Lett. **106**, 165005 (2011).

[12] W. Horton, G. T. Hoang, C. Bourdelle, X. Barbet, M. Ottaviani, and L. Colas, Phys. Plasmas **11,** 2600 (2004).

[13] V. Sokolov and A. K. Sen, Phys. Rev. Lett. **107,** 155001 (2011).

[14] L. M. Awasthi, S. K. Mattoo, R. Jha, R. Singh, and P. K. Kaw, Phys. Plasmas **17,** 042109 (2010).

[15] X. Wei, V. Sokolov, and A. K. Sen, Phys. Plasmas **17,** 042108 (2010).

[16] S. K. Mattoo, V. P. Anita, L. M. Awasthi, and G. Ravi, Rev. Sci. Instrum. **72,** 3864 (2001).

[17] Noah Hershkowitz, James R. DeKock, Peter Coakley, and Steven L. Cartier, Rev. Sci. Instrum. **51,** 64 (1980).

[18] J. Q. Dong, H. Sanuki, and K. Itoh, Phys. Plasmas **8,** 3635 (2001).

[19] S. C. Cowley, P. K. Kaw, R. S. Kelly, and R. M. Kulsrud, Phys. Fluids B **3,** 2066 (1991).

[20] R. Srinivasan, K. Avinash, and P. K. Kaw, Phys. Plasmas **8,** 4483 (2001).

[21] O. Motojima *et al.*, in *Proceedings of the 21st IAEA Fusion Energy Conference, Chengdu, China, 2006,* http://www-naweb.iaea.org/napc/physics/FEC/FEC 2006/html/node31.htm#5947, IAEA-CN-149/OV/2-1.

[22] H. A. B. Bodin and A. A. Newton, Nucl. Fusion **20,** 1255 (1980).

[23] R. A. Truemann, L. Brostrom, J. LaBelle, and N. Sckopke, J. Geophys. Res. **95,** 19 099 (1990).

[24] J. P. Boeuf, G. J. M. Hagelaar, P. Sarrailh, G. Fubiani, and N. Kohen, Plasma Sources Sci. Technol. **20,** 015002 (2011).